Chinese Chemical Letters 33 (2022) 3809–3817

Contents lists available at ScienceDirect

Chinese Chemical Letters

journal homepage: www.elsevier.com/locate/cclet

Catalytic degradation of lomefloxacin by photo-assisted persulfate activation on natural hematite: Performance and mechanism

Ruonan Guo, Ying Chen, Bingrui Liu, Ying Han, Jianfeng Gou*, Xiuwen Cheng*

Key Laboratory for Environmental Pollution Prediction and Control, Gansu Province, College of Earth and Environmental Sciences, Lanzhou University, Lanzhou 730000, China

ARTICLE INFO

Article history:
Received 27 July 2021
Revised 8 October 2021
Accepted 21 November 2021
Available online 26 November 2021

Keywords:
Natural hematite
Persulfate
Photocatalytic
Antibiotic degradation

ABSTRACT

The natural hematite (α-Fe_2O_3) is stable and abundant on the earth, as well as with strange electronic band structure and good visible light absorption properties. However, the composition and catalytic performance of natural hematite should be explored. In this study, the photo-assisted hematite nanoparticles activated persulfate (H-NPs/PS/vis) system was constructed. As detected, H-NPs had an irregular agglomerate structure with abundant internal pore and were mainly composed of Fe_2O_3, SiO_2 and TiO_2. The system was applied to removing various antibiotic (*i.e.*, lomefloxacin, ciprofloxacin and enrofloxacin with initial concentration of 10 mg/L), achieving high degradation performance of 82.0%, 81.2% and 82.2% after 120, 330 and 240 min, respectively. Moreover, H-NPs had excellent reusability with low metal leaching (Ti leaching percentage lower than 0.01%, Fe dissolution percentage was 0.48%) and stable structure. At last, a possible reaction mechanism of H-NPs/PS/vis system was proposed that lomefloxacin (LOM) was efficiently removed *via* the synergistic process of components contained in H-NPs with PS and light, involving the generation of $^{\bullet}O_2^-$, $^{\bullet}OH$ and $SO_4^{\bullet-}$. Above all, this paper provided a novel application scheme of natural hematite through in-depth and comprehensive experimental exploration.

Due to the irreplaceable role of antibiotics in disease treatment, antibiotics are more and more widely used in many fields [1]. The antibiotics are with high toxicity and negative environmental effects even at low concentrations [2,3], even lead to the existence of resistance genes [4]. However, antibiotics are unable to be completely metabolized by organisms, so that the traditional technologies are incapable of their efficient removal from urban sewage treatment [5,6]. Therefore, pharmaceutical and personal care products (PPCPs) have become a research hotspot because of their gradual accumulation in environment, so that various techniques have been developed for the treatment of wastewater which is contained of antibiotic drugs [7,8].

In traditional advanced oxidation processes (AOPs), hydrogen peroxide (H_2O_2) is used as oxidant to produce hydroxyl radical ($^{\bullet}OH$) for targeted pollutants removal. However, the instability of $^{\bullet}OH$ and its production efficiency are limited by narrow available pH range (2.8–3.5) [9,10]. Thus, in recent years, persulfate which can be activated to produce abundant powerful sulfate radical ($SO_4^{\bullet-}$) has been considered as a potential alternative oxidant for AOPs. Compared with $^{\bullet}OH$ (acid solution 2.7 V, neutral solution 1.8 V), $SO_4^{\bullet-}$ has a higher redox potential (2.5–3.1 V), better selectivity, longer half-life and wider pH tolerance range [11]. Therefore, sulfate radical-based AOPs (SR-AOPs) have been frequently applied to treat wastewater which contains recalcitrant and non-biodegradable contaminants. Among various methods for $SO_4^{\bullet-}$ generation, the use of heterogeneous nanocatalysts to activate persulfate has proved to be an effective strategy [12,13].

In order to improve the degradation efficiency of contaminants, UV/persulfate/transition metals catalyst (light-responsive photocatalyst) system has been further studied. Iron-based catalysts have been focused due to their high-efficient and low-toxicity [14]. Correspondingly, an innovative combination of visible light irradiation and heterogeneous iron oxide catalyst for AOPs has provided a prospective approach for the sustainable use of solar energy and iron species, while promoting the circulation efficiency of surface Fe(III)/Fe(II) *via* using light generated electrons [14–16]. Hematite not only has a strange electronic band structure, but also has good visible light absorption properties [14,17]. Recently, hematite has been wildly studied in AOPs counting on its abundance, accessibility and non-toxicity [18]. Nonetheless, the as-studied hematite nanoparticles were obtained through solvothermal and calcination methods [17,19,20], which are time consuming and energy intensive, and have high requirements on raw materials. Specifically,

* Corresponding authors.
E-mail addresses: goujf@lzu.edu.cn (J. Gou), chengxw@lzu.edu.cn (X. Cheng).

https://doi.org/10.1016/j.cclet.2021.11.061
1001-8417/

natural hematite (α-Fe_2O_3) is the most stable and abundant iron oxide on the earth. However, the composition and catalytic performance of natural hematite should be explored, as well as the reaction effect and mechanism of photo assisted persulfate activation system for pollutant degradation need to be further studied.

Overall, to explore the potential of natural hematite nanoparticles (H-NPs) in the field of environmental remediation, the physicochemical property of H-NPs would be detected, including micromorphology, composition and crystal phase structure. Moreover importantly, the photo-assisted hematite nanoparticles (H-NPs) activated persulfate (H-NPs/PS/vis) system would be constructed and used to remove nonbiodegradable organic pollutants in water. The effect of experimental parameters and co-existing substances on the system also need to be further detected. The contribution of reactive oxide species generated in H-NPs/persulfate/photocatalytic reaction system (H-NPs/PS/vis) would be investigated to prove the reaction mechanism. And then, with combination of characterization method, we would propose a possible reaction mechanism of efficient removal of refractory antibiotic pollutants in H-NPs/PS/vis system.

H-NPs were brought from Shandong analysis and test center. Lomefloxacin (LOM, $C_{17}H_{19}F_2N_3O_3$) was purchased from Aladdin Chemistry Co., Ltd. Besides, peroxydisulfate (PS, $K_2S_2O_8$), potassium hydroxide (KOH), sulfuric acid (H_2SO_4), potassium nitrate (KNO_3), potassium bicarbonate ($KHCO_3$), potassium chloride (KCl), humic acid (HA), *tert*–butyl alcohol (TBA, $C_4H_{10}O$), *p*-benzoquinone (*p*-BQ), potassium dichromate ($K_2Cr_2O_7$), ethylenediaminetetraacetic acid (EDTA) and ethanol (Et-OH, C_2H_5OH) were provided by Sinopharm Chemical Reagent Co., Ltd. Deionized water (DI water, resistivity of 13–15 MΩ cm) was used throughout this experiment. The chemicals in this experimental process were analytical grade and without further purification. As for characterization methods of catalyst, the JSM-5600LV scanning electron microscopy (SEM) with an EDS attachment was applied to detect microscopic morphology of H-NPs. The phase structure of catalysts was identified by a D/max-2004 Advance X-ray diffractometer (XRD) with a film attachment under Cu Kα radiation ($\lambda = 0.15418$ nm). And the applied current, accelerating voltage, step length and measurement speed were set as 40 mA, 40 kV, 0.02° and 0.1 s/step, respectively. X-ray photoelectron microscope (XPS) was carried out to determine the near-surface elements chemical states by a PHI-5700 ESCA apparatus (radiation source was monochromatic Al Kα radiation and pass energy was set as 1486.6 eV). In addition, The C 1s at 284.8 eV served as adventitious carbon used to calibrate the shift of binding energy [21]. Metal leaching of H-NPs in photo-assisted reaction systems was measured by Agilent 7700 ICP-MS. An electron paramagnetic resonance (EPR) spectrometer (Bruker A300–10/12) was used to determine the dominant reactive oxide species (*i.e.*, $^{\bullet}OH$, $SO_4^{\bullet-}$ and $^{\bullet}O_2^-$) in continuous wave X-band mode, which were captured by a spin trapping agent 5,5-dimethylpyrroline-oxide (DMPO).

In this study, LOM was selected as simulated pollutant and served as probing molecule to detect the PS activation performance of H-NPs. In experiments, 21.6 mg (0.8 mmol/L) PS and 5.0 mg H-NPs were put into a reactor of 100 mL 10 mg/L LOM solution. Afterwards, the suspension was exposed under a 35 W Xenon lamp (operating wavelength: 190–1100 nm, ± 1.0 nm) as an extra visible light source and magnetic stirring in the meantime. At a certain time interval, the water samples were got from the reactor and filtered *via* 0.22 μm nitrocellulose membrane. The results were determined *via* measuring the absorbance of LOM solution at 281 nm *via* ultraviolet-visible spectrophotometer. All of the experiments were proceeded at 30 °C. Moreover, to study the influence of pH in the above-mentioned photocatalysis system, 0.5 mol/L H_2SO_4 or KOH solutions was used to adjust from 3.00 to 13.00 before the adding of PS and H-NPs. Besides, a certain amount of relevant potassium salts and humic acid were put into the suspension solutions to identify the effect of co-existing substances. The system was employed to removal various antibiotics in water, and the concentration of contaminants was 10 mg/L totally. As the stability and repeatability are of great concern for the catalysts in practical applications. The photostability of H-NPs was assessed *via* cycling experiments under the same conditions to measure PS activation performance. After each run, the suspension was centrifuged to separate H-NPs powder, and then washed by Et-OH and DI water repeatedly to ensure completely removing coexisting ions and degradation intermediate. After that, adding the re-collection H-NPs into a new reaction cycle under identical experimental conditions. At last, putting the used H-NPs into oven and drying under 60 °C overnight, to complete SEM and XPS measurements for comparison to fresh H-NPs confirming the stability and repeatability of catalyst.

In this study, LOM was selected as a simulated pollutant to detect the PS activating capability of H-NPs in water, as shown in Fig. 1a. Firstly, the adsorption efficiency of H-NPs was detected as 16.3% within 120 min, but Xenon lamp irradiation was unable to destroy LOM molecules efficiently either. As well as, the removal of LOM was pretty low in single chemical oxidation and H-NPs/PS systems, illustrating that either H-NPs activating PS or PS alone could not decompose forming plenty reactive species to remove LOM efficiently. Nevertheless, with the addition of PS and Xenon lamp irradiation simultaneously, 82.0% LOM was destroyed in H-NPs/PS/vis system after 120 min treatment. In sharp contrast to the degradation efficiency of other reaction systems, implying that H-NPs/PS/vis system has a commendable performance for organic pollutants removal in water. Meanwhile, it was proved that catalyst, PS and visible light were indispensable in H-NPs/PS/vis system to destroy LOM efficiently. Compared with those artificially synthesized iron-based catalysts, H-NPs is an admirable catalyst with smaller risk of secondary contamination, lower health hazards, nature easy-gained and more negligible environmental influence. Therefore, H-NPs/PS/vis system has expansive application prospect in organic contaminants water treatment for further study.

In order to further confirm the practical application potential and universal applicability of H-NPs/PS/vis system, the degradation efficiencies of various quinolone antibiotics were detected in this system. LOM and ciprofloxacin (CIP) are traditional antibiotics applied for human treatment, while enrofloxacin (ERF) is a common animal therapy drug. These antibiotics pollution threatens aquatic ecosystems and water supplies. As reported, quinolone antibiotics have commonly been detected in multiple natural water bodies and even in sewage treatment plants [22]. Recent years, a variety of treatment technologies have been developed for the removal of antibiotics. As presented in Fig. 1b and Fig. S1 (Supporting information), all of the selected quinolones can be removed efficiently in H-NPs/PS/vis system. More than 80% LOM was degraded from water within 120 min. In addition, the as-constructed photo-assisted SR-AOPs also achieved 81.2% and 82.2% degradation efficiency of CIP and ERF after 330 and 240 min, respectively. Thus, H-NPs/PS/vis system had the ability to remove a variety of antibiotic contaminants in water, implying that H-NPs activating persulfate with assistance of light is a promising technique for the efficient removal of antibiotics.

It is important to confirm the stability and reusability of H-NPs for practical application. In this research, the consequence of photostability was detected by five cycling runs. Seen from Fig. 1c, the degradation efficiency of LOM was almost unchanged after five sequential cycles. Meanwhile, on account of H-NPs containing transition mental Fe and Ti, excessive metal leaching concentration would lead to secondary pollution in the degradation process which could affect the practical application potential of H-NPs/PS/vis system. Therefore, the dissolution concentration of tran-

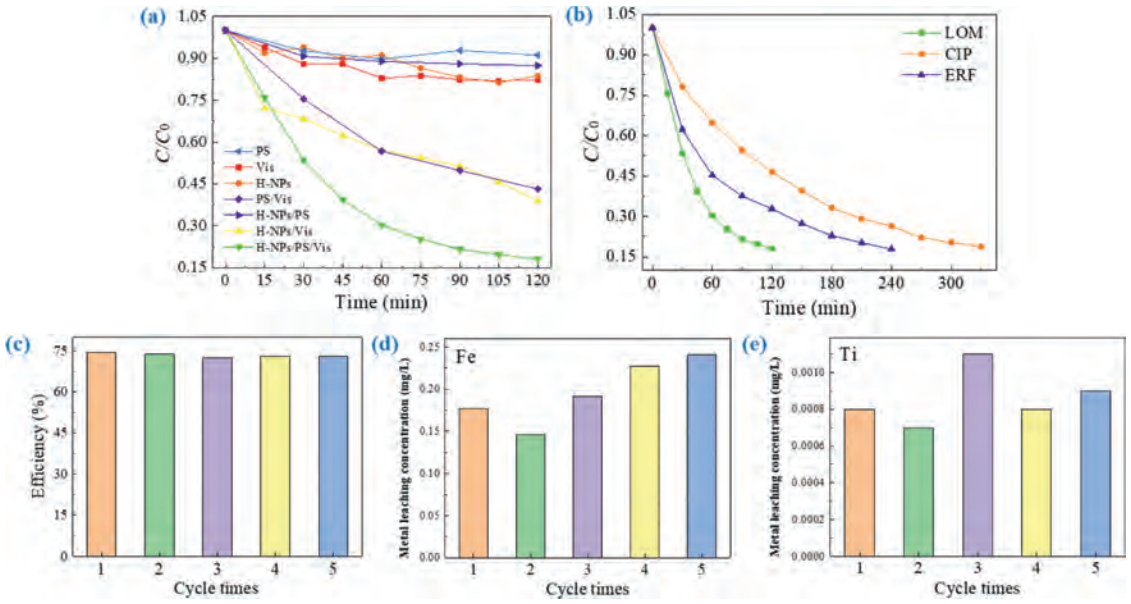

Fig. 1. (a) Removal of LOM in different reaction systems (reaction conditions: Solution volume = 50 mL, $[LOM]_0$ = 10 mg/L, $[PMS]_0$ = 0.8 mmol/L, $[H\text{-}NPs]_0$ = 50 mg/L, initial pH 5.98 (unadjusted) and reaction temperature = 30 °C). (b) Removal efficiency of different antibiotic drugs (reaction conditions: Solution volume = 50 mL, $[LOM]_0$ = 10 mg/L, $[PMS]_0$ = 0.8 mmol/L, $[H\text{-}NPs]_0$ = 50 mg/L, unadjusted initial pH and reaction temperature = 30 °C). (c) Degradation efficiency of LOM in recycle experiments and metal leaching of H-NPs/PS/vis system, the metal leaching concentration of (d) Fe and (e) Ti (reaction conditions: Solution volume = 50 mL, $[LOM]_0$ = 10 mg/L, $[PMS]_0$ = 0.8 mmol/L, $[H\text{-}NPs]_0$ = 50 mg/L, unadjusted initial pH and reaction temperature = 30 °C, reaction time = 40 min).

Table 1
Percentage of metal leaching in hematite/PS/vis system.

Cycling rus	1	2	3	4	5
Fe (%)	0.35%	0.29%	0.38%	0.45%	0.48%
Ti (%)	< 0.01%	< 0.01%	< 0.01%	< 0.01%	< 0.01%

sition metal ions in water samples during cycling runs was measured by ICP. Seem from Figs. 1d and e, the metal leaching concentration of H-NPs was pretty low. Moreover, the dissolution concentration of Ti ions was much lower than that of Fe ions, and the leached concentration of Fe ions presented an increasing trend in the augment of cycle times. Figuring out the corresponding percentage of metal ions dissolution which was the ratio of metal ions dissolution to the addition amount of H-NPs in this system displayed in Table 1.

Notably, Ti had the highest leaching percentage on the third time, but the percentage of Ti leaching was lower than 0.01%. Therefore, Ti ions leaching in H-NPs system could be ignored. At the meantime, the Fe ions leaching concentration achieved the maximum value of 0.2408 mg/L after five times, and dissolution percentage was 0.48% correspondingly. In conclusion, metal leaching concentration of transition metal in H-NPs/PS/vis system was pretty low. The heterogeneous system could effectively control the metal ions leaching concentration. Moreover, we compared this reaction system with another reported studies about iron-based nanocatalysts (Table S1 in Supporting information), illustrating that the H-NPs/PS/vis reaction system exhibited considerable application potential due to its advantages such as excellent and stable degradation performance, small amount of catalyst and oxidant, as well as pretty low metal leaching. Hence, it was a kind of green, economic and efficient photocatalytic system which was conducive to maintaining the stability of degradation efficiency and avoiding the secondary pollution of heavy metals.

Besides, as displayed in Figs. S2a and b (Supporting information), the change of H-NPs microstructure was insignificant. It could be observed from Figs. S2a and b that the SEM images of H-NPs presented a compact irregular stacked aggregate lump-shape with uneven surface and particle size as before after five cycles. It can be seen that the particles of different sizes were in a state of accumulation and agglomeration, whereas the internal aperture turned to be smaller. According to EDS spectrum exhibited in Fig. S2c (Supporting information), the main elements in H-NPs had not changed. Whereas, the content of Fe decreased, which were consistent with the elements content in above-discussed metal ion dissolution analysis. For natural raw H-NPs, the Fe ion leaching concentration was not too high with comparison of some artificial Fe-based catalysts [23,24]. This fact was attributed to that Fe existed in form of Fe_2O_3 with a tight agglomeration structure and the highest content. Hence, it was difficult to be separated from H-NPs surface during reaction process to reduce the occurrence of consumption. Fig. 2 exhibited the comparison of XPS spectra of H-NPs before and after five cycles. It could be seen from the full XPS spectra that there was almost no change in characteristic peak position of C, O, Si, Ti and Fe after the repeated reaction. Nevertheless, it could be observed that the peak intensity of Ti decreased dramatically. This fact may be ascribed to that LOM and intermediate products during experimental process were adsorbed on the surface of H-NPs and occupied active sites. Overall, the chemical elements contained in H-NPs remained well after five cycle experiments, in addition the microstructure was relatively stable with certain repeatability.

The micromorphology of H-NPs was further verified by SEM and presented in Figs. 2a and b. The SEM images indicated H-NPs had an irregular agglomerate structure with nonuniform particle sizes and rough surface. As displayed in Fig. S3 (Supporting information), most of the particle sizes were smaller than 200 nm accounting for over 80%, and between 1 nm to 100 nm were 40%–60% approximately. Moreover, H-NPs were with plentiful inner pore channels, which can further increase the local concentration of organic molecules in the vicinity of active layer, thus improving the reaction efficiency [25]. In the meanwhile, this microstructure can improve light collection efficiency by reflecting and scattering light multiple times in the voids inside of H-NPs, which is beneficial to photocatalysis [26]. Seen from Fig. S4 (Supporting informa-

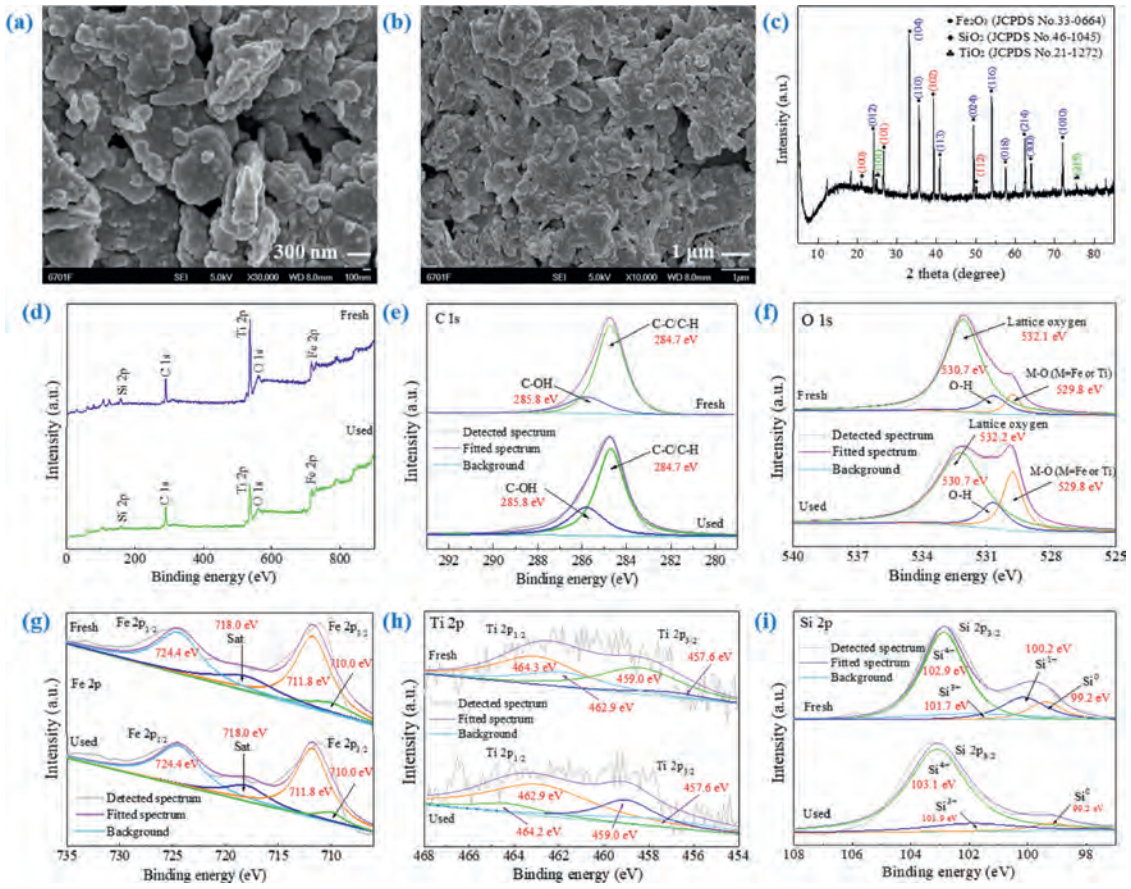

Fig. 2. (a, b) SEM images and (c) XRD patterns of H-NPs. (d) XPS spectra of H-NPs. High resolution XPS spectra of (e) C 1s, (f) O 1s, (g) Fe 2p, (h) Ti 2p and (i) Si 2p.

tion), EDS spectrum demonstrated that multifarious elements are co-existed in H-NPs and Fe signal is the uppermost. The atomic contents of Fe, Ti, Si and Al were quantified to be 32.24%, 0.33%, 1.03% and 0.49%, respectively. Among these elements, Ti is transition mental which is always applied to prepare photocatalysts [27]. Si could serve as inert nonmetallic element which was used as frozen composition of active substance in material preparation, as well as can play role in photocatalysis process [28]. Meanwhile, C and O accounted for big parts, implying that there may be abundant functional groups on the surface of H-NPs, which may be conducive to the decomposition of PS and adsorption of LOM.

The crystal structure of H-NPs was determined *via* XRD analysis with result shown in Fig. 2c. The main characteristic peaks in 24.14°, 33.17°, 35.65°, 40.86°, 49.47°, 54.07°, 57.59°, 62.45°, 64.02° and 71.95° were ascribed to (012), (104), (110), (113), (024), (116), (018), (214), (300) and (1010) lattice plane of Fe_2O_3 (PDF #33–0664). The intense peaks located at 20.88° (100), 26.62° (101), 39.28° (102) and 50.14° (112) confirmed the existence of SiO_2 (PDF #46–1045). Furthermore, the classic diffraction peaks at 24.89° and 75.47° were ascribed to lattice plane (101) and (215) of anatase TiO_2 (PDF #21–1272) which was the primary photosensitive crystal type to be helpful for enhancing photocatalytic capability of H-NPs [29,30]. Hence, XRD proved the well-defined crystal structure of H-NPs and further confirmed that H-NPs mainly contained Fe_2O_3, SiO_2 and anatase TiO_2, which were consistent with the elements mentioned in EDS analysis.

XPS spectra were recorded to confirm elements types and chemical valence on the surface of H-NPs. Clearly seen from Fig. 2d, the XPS full-survey spectrum exhibited obvious peaks of Si, Fe, Ti, O and C which was same as the analyses of EDS and XRD to prove the main elements of H-NPs adequately. More importantly, high resolution XPS spectra were applied to analyze element chemical states. As exhibited in Fig. 2e, the XPS spectrum of C 1s was composed of two characteristic peaks located in 284.7 eV and 285.8 eV which was corresponding to C-C/C-H and C-OH, respectively [31]. The three strong peaks in O 1s spectrum (Fig. 2f) at 529.8 eV, 530.7 eV and 532.1 eV were assigned to M-O (M = Fe or Ti), O-H and lattice oxygen [31]. This result indicated that the oxygen element in H-NPs mainly existed as above three states, which were identical to the results obtained from XRD analysis. Meanwhile, as depicted in Fig. 2g the high resolution XPS spectrum of Fe 2p was fitted with four peaks. According to previous researches, the two evident peaks at 710.0 eV and 711.8 eV were attributed to Fe $2p_{3/2}$, and the characteristic peak located at 724.4 eV was related to Fe $2p_{1/2}$. Combining with the satellite peak at 718.0 eV, iron element in H-NPs existed in the form of Fe_2O_3, because all above peaks were characteristic peaks of Fe_2O_3 [31]. Besides, there was no Fe^0 peak in the Fe 2p spectrum indicated that metallic iron was completely oxidized which demonstrated iron element in H-NPs was in the shape of metal oxides entirely [32]. In Fig. 2h, XPS spectrum of Ti 2p could be decomposed into four distinct peaks. The characteristic peaks of 459.0 eV ($2p_{3/2}$) and 464.3 eV ($2p_{1/2}$) were one group that proved the existence of Ti(IV). In addition, another group peaks of 457.6 eV ($2p_{3/2}$) and 462.9 eV ($2p_{1/2}$) were characteristic peaks of Ti(III) [33]. Moreover, the comparison of peaks showed that the characteristic peaks area of Ti(IV) was significantly larger than that of Ti(III). This fact implied that the most of titanium in H-NPs existing in Ti(IV) valence state, which was corresponded to the main composition TiO_2 confirmed by XRD spectrum. Furthermore, the Si 2p spectrum in Fig. 2i was decomposed into four peaks centered at 99.2 eV, 100.2 eV, 101.7 eV and 102.9 eV, which were related to Si $2p_{3/2}$ and regarded as the in-

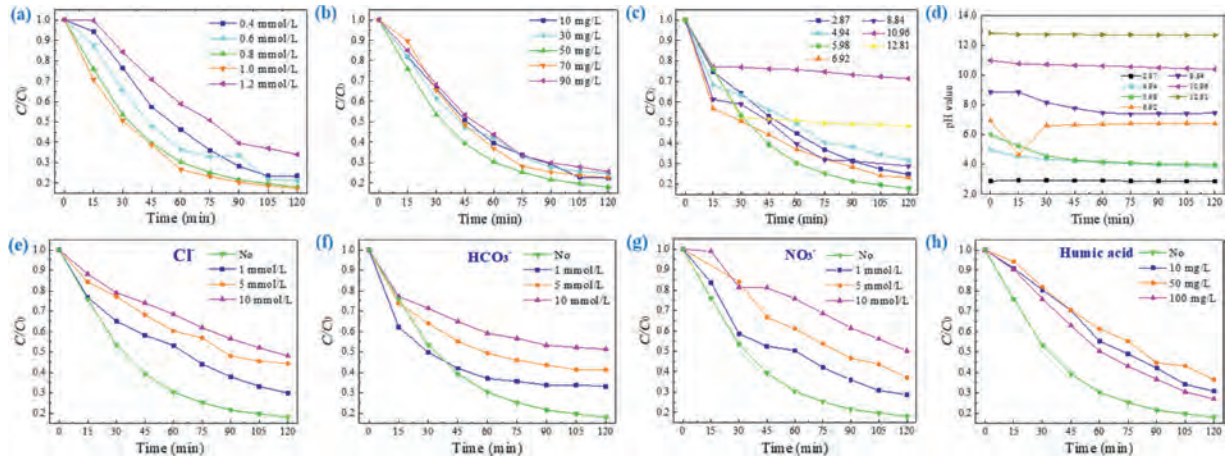

Fig. 3. (a) Influence of PS concentration (reaction conditions: Solution volume = 50 mL, $[LOM]_0$ = 10 mg/L, $[H\text{-}NPs]_0$ = 50 mg/L, initial pH and reaction temperature = 30 °C). (b) Influence of H-NPs dosage (reaction conditions: Solution volume = 50 mL, $[LOM]_0$ = 10 mg/L, $[PMS]_0$ = 0.8 mmol/L, initial pH and reaction temperature = 30 °C). (c) Influence of initial pH value and (d) pH value change (reaction conditions: Solution volume = 50 mL, $[LOM]_0$ = 10 mg/L, $[PMS]_0$ = 0.8 mmol/L, $[H\text{-}NPs]_0$ = 50 mg/L and reaction temperature = 30 °C). Influences of (e) Cl^-, (f) HCO_3^-, (g) NO_3^- and (h) humic acid on the degradation of LOM (reaction conditions: Solution volume = 50 mL, $[LOM]_0$ = 10 mg/L, $[PMS]_0$ = 0.8 mmol/L, $[H\text{-}NPs]_0$ = 50 mg/L, initial pH and reaction temperature = 30 °C).

dicator of Si, Si(I), Si(III) and Si(IV) [34,35]. Thereinto, the relevant peaks area followed order of Si(IV) > Si(I) > Si > Si(III), and the peak area of Si(IV) was much larger than that of another three valence states. It was demonstrated that Si element in H-NPs mainly existed as Si(IV), while having slight another valence silicon. This consequence was consistent with the conclusion that the main compound of silicon element appeared as SiO_2 obtained by XRD analysis.

It is well known that the generation of plentiful $SO_4^{\bullet-}$ and $^{\bullet}OH$ which play essential role in organic pollutant removal process. In general, the higher oxidant concentration would produce more $SO_4^{\bullet-}$ and $^{\bullet}OH$ to accelerate removal rate and enhance elimination efficiency. Thus, Fig. 3a and Fig. S5a (Supporting information) demonstrated the influence of PS concentration on LOM degradation efficiency and reaction rate constant, which was fit *via* the *pseudo*-first-order kinetic equation. With the change of PS concentration from 0.4 mmol/L to 0.8 mmol/L, LOM degradation efficiency and rate constants increased from 76.4% to 82.0% and 0.014 min^{-1} to 0.015 min^{-1}, respectively. Clearly, efficiency and rate constants were escalated with the increase of PS concentration (0.4 mmol/L, 0.6 mmol/L and 0.8 mmol/L). However, when the concentration of PS was higher than 0.8 mmol/L, experimental result reflected an inhibited and inefficient reaction effect. With initial PS concentration of 1.2 mmol/L, the efficiency and rate constant of reaction system reduced to 66.0% and 0.010 min^{-1}, respectively. As for explanation for this phenomenon, PS is regarded as the contributor of $SO_4^{\bullet-}$, therefore, enhancing appropriately of PS will encourage more $S_2O_8^{2-}$ to generate to attach the active sites on H-NPs surface which can promote LOM degradation process (Eq. 1) [36]. When PMS concentration remained too low to produce enough radical species, reaction rate would increase with PMS concentration, leading to an increased degradation efficiency as well as reaction rate. Whereas, higher PS concentration was, more reactive oxide species would be activated, so that the self-consume reactions of $SO_4^{\bullet-}$ and $S_2O_8^{2-}$ may occur (Eqs. 2 and 3) generating $S_2O_8^{\bullet-}$ and $S_2O_8^{2-}$ with poor reactive property and leading to lower LOM removal efficiency [37]. For another aspect, PS concentration could influence application cost as well as result in excessive salt concentration in water, which has a negative impact on the aquatic environment [38]. Hence, we selected 0.8 mmol/L as optimal PS concertation in this study.

$$S_2O_8^{2-} + vis/Catalyst \rightarrow 2SO_4^{\bullet-} \quad (1)$$

$$SO_4^{\bullet-} + SO_4^{\bullet-} \rightarrow S_2O_8^{2-} \quad (2)$$

$$SO_4^{\bullet-} + S_2O_8^{2-} \leftrightarrow S_2O_8^{\bullet-} + SO_4^{2-} \quad (3)$$

The relation between LOM degradation efficiency and H-NPs dosage is similar to influence of PS concentration. As depicted in Fig. 3b and Fig. S5b (Supporting information), when the dosage of H-NPs increased from 10 mg/L to 50 mg/L, both of LOM degradation efficiency and rate increased from 75.4% to 82.0% and from 0.012 min^{-1} to 0.015 min^{-1} correspondingly. This is due to that the higher photocatalyst dosage was, more improvable active sites would be existing to promote the production of photoinduced charge carriers and radicals. When H-NPs dosage increased to 70 mg/L and 90 mg/L, the enhancement of LOM degradation efficiency could not be observed, as well as the removal rate of LOM in H-NPs/PS/vis system. This fact can be explained that the excessive active sites with too much catalyst addition would lead to overmuch generated radicals, occurring self-scavenge reaction of $SO_4^{\bullet-}$ (Eq. 2). Additionally, for photocatalytic reaction system, the increased H-NPs dosage in suspension may lead to that a part of radiant energy of the incident light to be lost due to scattering [39]. As a result, photocatalytic actions for the catalyst and PS were limited, leading to a reduced LOM removal performance in H-NPs/PS/vis system. Consequently, 50 mg/L was selected as optimal catalyst dosage with consideration of LOM removal performance and economic cost.

In AOPs, pH is a primary influence factor that can impact the activation performance of catalyst and removal efficiency of targeted pollutants. Hence, the influence of initial pH on experimental process was detected under acidic (pH 2.87), weakly acidic (pH 4.94), unadjusted (pH 5.98), neutral (pH 6.92), weakly alkaline (pH 8.84) and alkaline (pH 10.96 and 12.81) conditions. Solution pH was not buffered to avoid the interference of buffering anions (*e.g.*, phosphate). As presented in Fig. 3c, the influence of initial solution pH on LOM removal in H-NPs/PS/vis system was significant. Nevertheless, LOM was rapidly and efficiently degraded in the wide pH range of 2.87–8.84. This reaction system was negatively affected under alkali conditions (pH 10.96 and 12.81), achieving the removal efficiencies of 51.7% and 28.6%, respectively. Because $SO_4^{\bullet-}$ exists in a solution with pH < 9 and predominates acidic conditions. However, sulfate radicals will transform to $^{\bullet}OH$ under strong

alkaline (Eq. 4) [40]. In addition, $^{\bullet}OH$ can be a quencher to consume $SO_4^{\bullet-}$ to influence the concentration of active substance (Eq. 5) [37]. Moreover, according to the measurement of pH changes (Fig. 3d), this system almost kept the initial pH value. Hence, the reaction results under alkaline condition exhibited worse than others, attributing to the poorer oxidation property and shorter lifetime of $^{\bullet}OH$ compared with $SO_4^{\bullet-}$. Under neutral and weakly alkaline, the coexistence of $^{\bullet}OH$ and $SO_4^{\bullet-}$ could accelerate degradation by participating together.

$$SO_4^{\bullet-} + OH^- \rightarrow {}^{\bullet}OH + SO_4^{2-} \quad (4)$$

$$SO_4^{\bullet-} + {}^{\bullet}OH \rightarrow HSO_5^- \quad (5)$$

The H-NPs/PS/Vis reaction system exhibited excellent LOM removal performance when initial pH in 2.87-8.84, particularly under the weakly acidic and neutral conditions. On account of most of natural water pH being from 5.0 to 9.0, the H-NPs/PS/vis reaction system can be fitted to apply in actual water treatment perfectly.

In general, natural water environment universally has abundant co-existing substances such as inorganic matters (Cl^-, HCO_3^- and NO_3^-) and natural organic matters like humic acid. These ingredients may affect the targeted contaminant removal process *via* reacting with reactive oxide species. To evaluate the pollutant degradation potential of H-NPs/PS/vis system in practical wastewater, detecting the influence of these natural matters with different concentration is significative.

As displayed in Fig. 3e and Fig. S6a (Supporting information), with the increase of Cl^- concentration from 1 mmol/L to 10 mmol/L, LOM removal efficiency changed from 70.1% to 51.9% and degradation rate constant reduced from 0.010 min^{-1} to 0.006 min^{-1}. Clearly, the presence of Cl^- played a significant inhibitory role in this photo-activated SR-AOP oxidation systems. On contrast to no-added system, the minimum change of degradation efficiency and rate constant was 11.9% and 0.005 min^{-1} with lower Cl^- concentration. In reaction process, Cl^- can react with $^{\bullet}OH$ and $SO_4^{\bullet-}$ to produce $HOCl^{\bullet-}$ and $Cl^{\bullet}$ correspondingly (Eqs. 6 and 8). Furthermore, $HOCl^{\bullet-}$ and H^+ will engender Cl^- to build a circulation which would expend $^{\bullet}OH$ constantly (Eq. 7). As for chlorine radicals, they are with inferior redox potential thereby reducing the concentration of $SO_4^{\bullet-}$ (Eq. 9) [37,41]. When the concentration of Cl^- was 5 mmol/L and 10 mmol/L, more chlorine radicals were generated and participated in the reverse reaction, while there were not enough $^{\bullet}OH$ and $SO_4^{\bullet-}$, which had strong oxidation capability. As a result, the degradation performance of LOM decreased.

$$Cl^- + {}^{\bullet}OH \rightarrow HOCl^{\bullet-} \quad (6)$$

$$HOCl^{\bullet-} + H^+ \rightarrow Cl^- + H_2O \quad (7)$$

$$Cl^- + SO_4^{\bullet-} \rightarrow Cl^{\bullet} + SO_4^{2-} \quad (8)$$

$$Cl^{\bullet} + Cl^- \rightarrow Cl_2^{\bullet-} \quad (9)$$

Seen from Fig. 3f and Fig. S6b (Supporting information), HCO_3^- performed an inhibitory effect in line with its induced concentration enhancement in H-NPs/PS/vis reaction system. With the addition of HCO_3^-, LOM removal efficiency decreased from 82.0% to 66.8%, 58.7% and 48.6%. Simultaneously, the rate constant declined from 0.015 min^{-1} to 0.008 min^{-1}, 0.007 min^{-1} and 0.005 min^{-1}. As reported, HCO_3^- can react with $^{\bullet}OH$ and $SO_4^{\bullet-}$ consuming these reactive radicals (Eqs. 10 and 11), so that the LOM degradation reaction was trapped [42].

$$HCO_3^- + {}^{\bullet}OH \rightarrow CO_3^{\bullet-} + H_2O \quad (10)$$

$$HCO_3^- + SO_4^{\bullet-} \rightarrow HCO_3^{\bullet-} + SO_4^{2-} \quad (11)$$

The influence of NO_3^- was conducted under NO_3^- concentration range from 1 mmol/L to 10 mmol/L, as presented in Fig. 3g and Fig. S6c (Supporting information). The experimental result confirmed the negative impact of NO_3^- in H-NPs/PS/vis system. The maximal inhibiting effect appeared in 10 mmol/L with degradation efficiency of 49.8% which decreased by 32.2%, meanwhile, the removal rate constant was reduced from 0.015 min^{-1} to 0.006 min^{-1}. Although $^{\bullet}OH$ could be motivated by the photolysis of NO_3^- (Eqs. 12 and 13), synchronously, NO_2^- would generate and react with $^{\bullet}OH$ and $SO_4^{\bullet-}$ as radical scavenger. Correspondingly, organic contaminant oxidation reaction was retarded (Eqs. 14 and 15). Besides, NO_3^- can directly scavenge $SO_4^{\bullet-}$ inhibiting removal of LOM (Eq. 16) [43,44].

$$NO_3^- \rightarrow \left[NO_3^-\right]^* \quad (12)$$

$$\left[NO_3^-\right]^* \rightarrow NO_2^{\bullet} + O^{\bullet-} \rightarrow NO_2^{\bullet} + {}^{\bullet}OH + OH^- \quad (13)$$

$$NO_2^- + {}^{\bullet}OH \rightarrow NO_2^{\bullet} + OH^- \quad (14)$$

$$NO_2^- + SO_4^{\bullet-} \rightarrow NO_2^{\bullet} + SO_4^{2-} \quad (15)$$

$$NO_3^- + SO_4^{\bullet-} \rightarrow NO_2^{\bullet} + SO_4^{2-} \quad (16)$$

Humic acid is one of representative natural organic matters in water environment. As depicted in Fig. 3h and Fig. S6d (Supporting information), the degradation efficiency and rate constant dropped significantly with comparison of original H-NPs/PS/vis system, proving that humic acid played inhibitory effect on LOM degradation process. Nevertheless, compared with the influence of inorganic matters (Cl^-, $HCO_3^-$and NO_3^-) in this study, the inhibitory effect of humic acid was weaker. According to previous study, lots of non-selective active substance, *i.e.*, $^{\bullet}OH$, would be consumed by humic acid, meanwhile, $SO_4^{\bullet-}$ could react with LOM molecules. Specially, when the concentration of humic acid increased to 100 mg/L, LOM removal efficiency was higher than those systems with another two concentrations (10 mg/L and 50 mg/L). This phenomenon can be explained that certain types of humic substances are photosensitive, and the increase of humic acid can provide more reaction sites for pollutant molecules and H-NPs. So that humic acid with a certain concentration may have a synergistic effect on contaminant degradation reaction in photocatalytic system [21,39]. Moreover, humic acid can enhance turbidity in suspension solution resulting in radiation energy scattering, so that the photo-activation process of PS would be hampered. In the meantime, humic acid competed with LOM molecules by capturing $^{\bullet}OH$ and $SO_4^{\bullet-}$ to hinder the LOM removal (Eqs. 17 and 18) [45]. In conclusion, with humic acid addition, LOM removal was greatly inhibited *via* multiple ways in H-NPs/PS/vis system.

$$\text{Humic acid} + SO_4^{\bullet-} \rightarrow \text{products} \quad (17)$$

$$\text{Humic acid} + {}^{\bullet}OH \rightarrow \text{products} \quad (18)$$

It was necessary to distinguish the main reactive oxide species for LOM degradation in H-NPs/PS/vis system. Commonly, $SO_4^{\bullet-}$ and $^{\bullet}OH$ could be generated *via* persulfate activation, in the meantime, $^{\bullet}O_2^-$ may be produced. The assistance of light irradiation led to the formation of photogenerated electrons (e^-) and holes (h^+), which can induce contaminant decomposition. The reaction rates of Et-OH/$^{\bullet}OH$ ($k = 9.1 \times 10^6$ L $mol^{-1}s^{-1}$) and Et-OH/$SO_4^{\bullet-}$ ($k = 3.5 \times 10^7$ L $mol^{-1}s^{-1}$) are close to each other [46]. TBA was selected as an

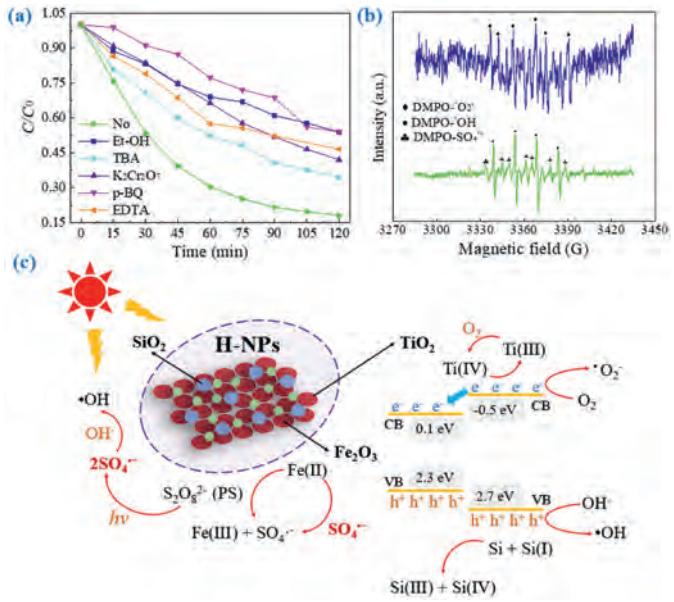

Fig. 4. (a) Removal efficiency of radical scavengers on the degradation of LOM by H-NPs/PS/vis system (reaction conditions: Solution volume = 50 mL, $[LOM]_0 = 10$ mg/L, $[PMS]_0 = 0.8$ mmol/L, $[H\text{-}NPs]_0 = 50$ mg/L, initial pH and reaction temperature = 30 °C). (b) EPR spectra in various reactions (reaction conditions: 35 W Xenon lamp, $[PMS]_0 = 0.8$ mmol/L, $[H\text{-}NPs]_0 = 50$ mg/L, initial pH and reaction temperature = 30 °C, LOM was not added). The possible reaction mechanism in H-NPs/PS/vis system.

$^{\bullet}OH$ scavenger ($3.8–7.6 \times 10^8$), because of the higher reaction activity with $^{\bullet}OH$ compared with $SO_4^{\bullet-}$ [47]. As shown in Fig. 4a, LOM degradation efficiency showed significant decrease during reaction processes with individual addition of TBA and Et-OH, illustrating that $^{\bullet}OH$ and $SO_4^{\bullet-}$ were played important roles in LOM degradation process. Moreover, *p*-BQ, $K_2Cr_2O_7$ and EDTA were applied to capture $^{\bullet}O_2^-$, photoinduced e^- and h^+, respectively. As shown in Fig. 4a, the addition of different scavengers caused an adverse effect on the degradation of LOM, and the adverse effect of *p*-BQ was more remarkable. This fact revealed that photoinduced e^- and h^+ contributed to LOM decomposition, particularly, $^{\bullet}O_2^-$ played essential roles in LOM degradation process.

Moreover, to identify the reactive radicals directly, EPR trapping experiments with DMPO were conducted. Seen from Fig. 4b, the signals of DMPO-$^{\bullet}O_2^-$ were detected. Besides, a four-line (1:2:2:1) spectrum (DMPO-$^{\bullet}OH$) appeared, as presented in Fig. 4b, indicating that H-NPs with assistance of light irradiation was able to activate PS producing $^{\bullet}OH$. Meanwhile, the relatively weak EPR signals of DMPO-$SO_4^{\bullet-}$ could be observed, indicating that $^{\bullet}OH$ was more important for LOM degradation process over than $SO_4^{\bullet-}$. In H-NPs/PS/vis system, the photocatalytic treatment and PMS activation act synergistically to produce a large amount of $^{\bullet}OH$ based on the reactions described in Eqs. 19 and 20 [48].

$$2SO_4^{\bullet-} + OH^- \rightarrow SO_4^{2-} + {}^{\bullet}OH \quad (19)$$

$$2SO_4^{\bullet-} + H_2O \rightarrow SO_4^{2-} + {}^{\bullet}OH + H^+ \quad (20)$$

Above all, $^{\bullet}OH$, $SO_4^{\bullet-}$ and $^{\bullet}O_2^-$ made predominant oxidation contribution in H-NPs/PS/vis system which produced on surface of catalyst. The photogenerated charge carriers played oxidization roles in the photo-assisted SR-AOPs as well. According to the above-mentioned analysis, a possible reaction mechanism of H-NPs/PS/vis system for organic contaminant degradation were proposed and depicted in Fig. 4c.

First of all, the chemical bonds of organic pollutants absorbed energy from light source and would be destroyed directly. Moreover, PS was activated by light irradiation to produce $SO_4^{\bullet-}$. According to previous research, O-O bond energy in PS (140.0 kJ/mol) was less than that in H_2O_2 (213.3 kJ/mol), thus, PS was more easily to be activated in photocatalysis system [21]. And the chemical bonds of pollutants were destructed by radicals achieving the purpose of organic pollutants degradation.

Secondly, based on the analysis of characterization, H-NPs were composed by Fe_2O_3, SiO_2 and TiO_2. It is widely accepted that TiO_2 was a traditional semiconductor with high photoactivity, splendid chemical inertia, low cost, non-toxicity and excellent sustainability [49]. As well, hematite (α-Fe_2O_3) frequently has been promoted as photocatalyst with favorable optical band gap (~2.1 eV) and excellent chemical stability [50]. The photocatalyst contained TiO_2 and Fe_2O_3 could produce photogenerated e^- and h^+ pairs efficiently with Xenon lamp irradiation (Eq. 21) and further induce the generation of various reactive oxide species, including $^{\bullet}OH$ and $^{\bullet}O_2^-$ (Eqs. 23 and 24). However, the limited solar light adsorption and high rate recombination of photogenerated carriers in pristine TiO_2 and α-Fe_2O_3 hinder their industrial and real-life applications. The composition of TiO_2 and α-Fe_2O_3 would adjust band gap so that H-NPs possessed more suitable band gap for visible light response and lower reduced charge carrier recombination rates (Eq. 22). Previous research proved that the absorbance of photocatalyst would increase with more Ti(III), which might promote TiO_2 to have preferable photocatalytic activity [51]. According to Eqs. 25 and 26, Ti(III) facilitated the production of $^{\bullet}O_2^-$ to accelerate the removal of pollutants [52]. Besides, as depicted in Fig. 2h, both of the characteristic peaks located at 462.9 eV and 464.2 eV were corresponded to Ti(III) and Ti(IV), respectively. After five cycles, Ti(III) increased and Ti(IV) decreased obviously, indicating the transformation of titanium from Ti(IV) to Ti(III). Therefore, this result indicated that a large amount of $^{\bullet}O_2^-$ was generated in this system based on the change from Ti(IV) into Ti(III). Corresponding to the experiment of free radical capture, $^{\bullet}O_2^-$ played essential roles in LOM degradation process in the H-NPs/PS/Vis system. More interestingly, PS could serve as an electron acceptor of photogenerated e^- reducing the recombination of e^- and h^+ (Eq. 27) [40].

$$\text{photocatalyst} + h\nu \rightarrow e^- + h^+ \quad (21)$$

$$e^-(TiO_2) \rightarrow e^-(Fe_2O_3) \quad (22)$$

$$O_2 + e^-\ (TiO_2) \rightarrow {}^{\bullet}O_2^- \quad (23)$$

$$OH^- + h^+ \rightarrow {}^{\bullet}OH \quad (24)$$

$$Ti(IV) + e^- \rightarrow Ti(III) \quad (25)$$

$$Ti(III) + O_2 \rightarrow Ti(IV) + {}^{\bullet}O_2^- \quad (26)$$

$$S_2O_8^- + e^-\ (Fe_2O_3/TiO_2) \rightarrow SO_4^{\bullet-} + SO_4^{2-} \quad (27)$$

Thirdly, the transition metal Fe with lower valence could also efficiently activate PS (Fenton-like process). In the heterogeneous system, the interaction between various iron species with different valence states would produce reactive oxide species in SR-AOPs (Eqs. 28 and 29) [53]. To better understand the catalytic mechanism of H-NPs for PS activation with assistance of UV-vis irradiation, the Fe 2p high resolution XPS spectra of fresh and used H-NPs were detected. The characterization result revealed that iron existed in form of Fe_2O_3 in H-NPs Fe 2p (Fig. 2g) and transformed slightly after repeated experiment. Thus, Fe(II) and Fe(III) were recycled and not consumed in the reaction process. Correspondingly,

Fe could activate PS to generate reactive species continuously while undergoing cyclic transformation process to maintain the stable catalyst performance of H-NPs.

$$Fe(II) + S_2O_8^{2-} \rightarrow Fe(III) + SO_4^{\bullet -} + SO_4^{2-} \quad (28)$$

$$Fe(III) + SO_4^{\bullet -} \rightarrow Fe(II) + SO_4^{2-} \quad (29)$$

According to relevant reports, the effect of SiO_2 composition on structure stability and photocatalytic reactivity of photocatalysts was determined [54,55]. Meanwhile, SiO_2 can immobilize nano-TiO_2 and Fe_2O_3 on its surface, preventing active sites aggregation and weakening the photoinduced carriers recombination to promote photocatalysis reaction on the surface of H-NPs [56]. At the same time, previous studies illustrated that due to the electron interaction between TiO_2 and Fe_2O_3, the composited photocatalysts would be with specific photolysis characteristics which affects the stability and photocatalysis. The introduction of SiO_2 could inhibit direct electrical contact at the interface of TiO_2 and Fe_2O_3, preventing the occurrence of light dissolution and strengthening the material stability and removal effect of antibiotic drugs [57]. On the other hand, amorphous SiO_2 can act as a role of absorbent to concentrate organic molecules near the active sites [25]. In this case, e^- and h^+ would be excited constantly inducing more different kinds of reactive species. In this process, oxygen atoms in the material were released to form oxygen holes, as following, water molecules took up these oxygen holes to produce –OH groups attaching to the surface of H-NPs. So that the surface of H-NPs was hydrophilic which was conducive to the efficient combination of catalyst material, oxidant and pollutant, improving the LOM removal efficiency. Fig. 2i depicted the transformation of Si state, in detail, the mass percent of Si^0 reduced and even the characteristic peak of Si(I) disappeared. Simultaneously, the contents of Si(III) and Si(IV) increased indicating that Si in H-NPs was converted from Si(I) and Si to Si(III) and Si(IV). As SiO_2 was a fixed material in H-NPs and a large area contacted reactive oxide substances, which might have influence on Si leading to the transformation of Si(I) and Si^0 into Si(III) and Si(IV).

Above all, LOM was efficiently removed *via* the synergistic process of components contained in H-NPs with PS and light. The composition of TiO_2 and Fe_2O_3 enhanced photocatalytic capability of H-NPs, promoting the occurrence of multiple light intensification reactions. Simultaneously, transition metals activated PS to produce abundant radicals with the assistance of light irradiation. Furthermore, SiO_2 provided an excellent structure and interface predominance for catalytic and oxidic reactions. Hence, H-NPs could be applied as catalysts without modified treatment in photo-assisted SR-AOPs to degrade antibiotic pollutants efficiently.

All in all, H-NPs/PS/vis system was applied to degrade LOM in this work. Firstly, based on characterization results, it was proved that H-NPs was mainly composed of Fe_2O_3, TiO_2 and SiO_2. Meanwhile, SEM images of H-NPs depicted the irregular block-shaped stacked and agglomerated microstructure with abundant pores, which was beneficial to adsorption of pollutant molecules and PS during the degradation process. Secondly, the pollutant degradation capacity of H-NPs/PS/vis system (82%, 120 min) were evaluated with comparison of various LOM degradation process. Additionally, the influence of different experiment parameters and co-existing ions were studied. It should be highlighted that the H-NPs/PS/vis system exhibited excellent degradation performance in various antibiotics removal process. As well, the results of repeated experiments and metal ion dissolution indicated that H-NPs had a good stability and low secondary contamination risk during LOM degradation process. Meanwhile, quenching experiments and common free radical quantitative concentration experiments clarify that $^{\bullet}O_2^-$, $^{\bullet}OH$ and $SO_4^{\bullet -}$ were the dominant reactive species in H-NPs/PS/vis system. Finally, a possible reaction mechanism was proposed based on the analysis characterization and experimental results, suggesting that LOM was efficiently removed *via* the synergistic process of components contained in H-NPs with PS and light. Therefore, H-NPs are an environment-friendly material suitable for photocatalysis as causing smaller risk of secondary contamination and more affordable.

Declaration of competing interest

We have no conflicts of interest to declare.

Acknowledgments

This work was kindly funded by National Natural Science Foundation of China (No. 51978319), Outstanding Youth Foundation of Gansu Province (No. 20JR10RA651) and Natural Science Foundation of Gansu Province (No. 20JR10RA635).

Supplementary materials

Supplementary material associated with this article can be found, in the online version, at doi:10.1016/j.cclet.2021.11.061.

References

[1] H. Zhan, Y. Wang, X. Mi, et al., Chin. Chem. Lett. 31 (2020) 2843–2848.
[2] J. Qi, J. Liu, F. Sun, et al., Chin. Chem. Lett. 32 (2021) 1814–1818.
[3] Z. Wu, Y. Wang, Z. Xiong, et al., Appl. Catal. B: Environ. 277 (2020) 119136.
[4] M. Wang, H. Liu, X. Dai, Environ. Pollut. 256 (2020) 113392.
[5] M. Zhang, J. He, Y. Chen, et al., Chin. Chem. Lett. 31 (2020) 2721–2724.
[6] L.J. Zhou, P. Han, M. Zhao, et al., Water Res 196 (2021) 117003.
[7] I.C. Iakovides, I. Michael-Kordatou, N.F.F. Moreira, et al., Water Res. 159 (2019) 333–347.
[8] M. Pan, T. Lyu, L. Zhan, et al., Water Res. 190 (2021) 116735.
[9] Y. Ahmed, J. Zhong, Z. Yuan, et al., Water Res. 197 (2021) 117075.
[10] C. Zhou, H. Zhou, Y. Yuan, et al., Chem. Eng. J. 420 (2021) 130370.
[11] R. Guo, Y. Li, Y. Chen, et al., Chem. Eng. J. 417 (2021) 127887.
[12] J. Lee, U. von Gunten, J.H. Kim, Environ. Sci. Technol. 54 (2020) 3064–3081.
[13] Q. Yang, Y. Ma, F. Chen, et al., Chem. Eng. J. 378 (2019) 122149.
[14] T. Guo, L. Jiang, H. Huang, et al., J. Hazard. Mater. 416 (2021) 125838.
[15] H. Jin, X. Tian, Y. Nie, et al., Environ. Sci. Technol. 51 (2017) 12699–12706.
[16] P. Avetta, A. Pensato, M. Minella, et al., Environ. Sci. Technol. 49 (2015) 1043–1050.
[17] T. Guo, L. Jiang, K. Wang, et al., Appl. Catal. B: Environ. 286 (2021) 119883.
[18] A.H. Asif, S. Wang, H. Sun, Curr. Opin. Green Sustain. Chem. 28 (2021) 100447.
[19] G. Li, C. Wang, Y. Yan, et al., Chem. Eng. J. 386 (2020) 124007.
[20] M. Guo, Z. Xing, T. Zhao, et al., Appl. Catal. B: Environ. 272 (2020) 118978.
[21] R. Guo, Y. Wang, J. Li, et al., Appl. Catal. B: Environ. 278 (2020) 119297.
[22] Y. Zhang, M. Xu, X. Liu, et al., Bioresour. Technol. 326 (2021) 124780.
[23] L. Li, Q. Zhang, Y. She, et al., Sep. Purif. Technol. 270 (2021) 118770.
[24] M. Cai, Y. Zhang, C. Dong, et al., J. Hazard. Mater. 405 (2021) 124228.
[25] C. Anderson, A.J. Bard, J. Phys. Chem. B 101 (1997) 2611–2616.
[26] G. Liao, S. Chen, X. Quan, et al., Appl. Catal. B: Environ. 102 (2011) 126–131.
[27] R. Li, W. Zhang, K. Zhou, Adv. Mater. 30 (2018) 1705512.
[28] S.W. Boettcher, E.L. Warren, M.C. Putnam, et al., J. Am. Chem. Soc. 133 (2011) 1216–1219.
[29] R. Guo, G. Zhu, Y. Gao, et al., Sep. Purif. Technol. 226 (2019) 315–322.
[30] Q. Ma, H. Zhang, R. Guo, et al., Electrochim. Acta 283 (2018) 1154–1162.
[31] G.F. Moreira, E.R. Peçanha, M.B.M. Monte, et al., Miner. Eng. 110 (2017) 96–103.
[32] P. Kaspar, D. Sobola, R. Dallaev, et al., Appl. Surf. Sci. 493 (2019) 673–678.
[33] S.A. Abdullah, M.Z. Sahdan, N. Nayan, et al., Mater. Lett. 263 (2020) 127143.
[34] S.P. Chenakin, G. Melaet, R. Szukiewicz, et al., J. Catal. 312 (2014) 1–11.
[35] K.Y. Pan, Y.F. Liang, Y.C. Pu, et al., Appl. Surf. Sci. 311 (2014) 399–404.
[36] M.Y. Lee, W.L. Wang, Z.B. Xu, et al., Sci. Total Environ. 655 (2018) 1261–1269.
[37] X. Liu, Y. Liu, S. Lu, et al., Chem. Eng. J. 385 (2020) 123987.
[38] R. Guo, L.-c. Nengzi, Y. Chen, et al., Chem. Eng. J. 398 (2020) 125676.
[39] R. Guo, Y. Chen, L.-c. Nengzi, et al., Chem. Eng. J. 398 (2020) 125556.
[40] F. Chen, G.X. Huang, F.B. Yao, et al., Water Res. 173 (2020) 115559.
[41] R. Guo, Y. Zhu, X. Cheng, et al., J. Hazard. Mater. 399 (2020) 122966.
[42] Y. Qian, X. Guo, Y. Zhang, et al., Environ. Sci. Technol. 50 (2016) 772–781.
[43] M.B. Ahmed, J.L. Zhou, H.H. Ngo, et al., J. Hazard. Mater. 323 (2017) 274–298.
[44] Y. Pan, M. Zhou, Y. Zhang, et al., Sep. Purif. Technol. 203 (2018) 66–74.
[45] M. Xu, J. Li, Y. Yan, et al., Chem. Eng. J. 369 (2019) 403–413.
[46] L. Lai, J. Yan, J. Li, et al., Chem. Eng. J. 343 (2018) 676–688.
[47] Y. Zhou, J. Jiang, Y. Gao, et al., Environ. Sci. Technol. 49 (2015) 12941–12950.
[48] A. Wang, H. Wang, H. Deng, et al., Appl. Catal. B: Environ. 248 (2019) 298–308.
[49] R. Guo, L.C. Nengzi, Y. Chen, et al., Chin. Chem. Lett. 31 (2020) 2661–2667.
[50] Y. Fu, C.L. Dong, W. Zhou, et al., Appl. Catal. B: Environ. 260 (2020) 118206.
[51] S. Wei, S. Ni, X. Xu, Chinese J. Catal. 39 (2018) 510–516.

[52] B. Zhang, A. Nakajima, M. Kiuchi, CIRP Ann.-Manuf. Technol. 51 (2002) 259–262.
[53] H. Li, J. Wan, Y. Ma, et al., Chem. Eng. J. 237 (2014) 487–496.
[54] Q. Jiang, J. Huang, B. Ma, et al., Colloids Surf. A 602 (2020) 125112.
[55] D. Cani, J.C. van der Waal, P.P. Pescarmona, Appl. Catal. A 621 (2021) 118179.
[56] C. Feng, Y. Xie, J. Zhao, et al., Chemosphere 44 (2001) 1159–1168.
[57] S. Zhang, J. Yi, J. Chen, et al., Chem. Eng. J. 380 (2020) 122583.